Electromagnetic probes in heavy-ion collisions

Raphaelle Bailhache[1,*]

[1]Goethe-Universität, Max-von-Laue-Strasse 1, 60438 Frankfurt am Main, Germany

Abstract. Electromagnetic probes such as photons and dileptons (l^+l^-) are a unique tool to study the space-time evolution of the hot and dense matter created in heavy-ion collisions, since they are emitted at all stages of the collision with negligible final-state interactions. In this article, the latest results on soft photon (real and virtual) production in heavy-ion collisions are presented.

1 Introduction

Electromagnetic probes such as photons and dileptons (l^+l^-) provide unique insights into the properties of the hot and dense matter created in heavy-ion collisions. They are emitted at all stages of the collision with negligible final-state interactions, unlike hadrons. Therefore, they carry undistorted information about space-time evolution of the medium. Direct real and virtual photons ($\gamma, \gamma^* \rightarrow l^+l^-$) are emitted by various sources. Prompt γ, γ^*s produced in initial hard scatterings provide a way to test $N_{\rm coll}$-scaling and constrain the nuclear parton distribution functions (PDFs). Pre-equilibrium γ, γ^*s, still generated before the system reaches local equilibrium, give insight into the mechanisms of equilibration. Thermal γ, γ^*s emitted from the quark-gluon plasma (QGP) and hot hadronic matter shed light on the temperature of the medium and its space-time evolution. Finally, dileptons originating from ρ mesons produced in the hot hadronic matter, where chiral symmetry is expected to be partially restored, are sensitive to mechanisms of chiral symmetry restoration.

2 Direct photons with low transverse momentum

Each source of direct photons populates different transverse momentum ($p_{\rm T}$) regions [1]. Prompt direct photons dominate at high $p_{\rm T}$ ($p_{\rm T} > 5\,{\rm GeV}/c$). Thermal photons are expected to contribute significantly for $p_{\rm T} < 2\text{-}3\,{\rm GeV}/c$ with an approximately exponential $p_{\rm T}$ spectrum, whose inverse slope parameter $T_{\rm eff}$ contains information on the medium temperature, although affected by radial flow. Pre-equilibrium γs may play a role at intermediate $p_{\rm T}$.

2.1 Status before QM 2023

PHENIX [2, 3] and STAR [4] at RHIC, as well as ALICE [5, 6] at the LHC, measured direct photons down to low $p_{\rm T}$ ($p_{\rm T} \approx 0.5\,{\rm GeV}/c$) in heavy-ion collisions employing different methods. An excess of direct γs is observed for $p_{\rm T} \leq 4\,{\rm GeV}/c$ compared to the expected contribution of prompt γs estimated from pp collisions or pQCD calculations, as can be seen

*e-mail: raphaelle.bailhache@cern.ch

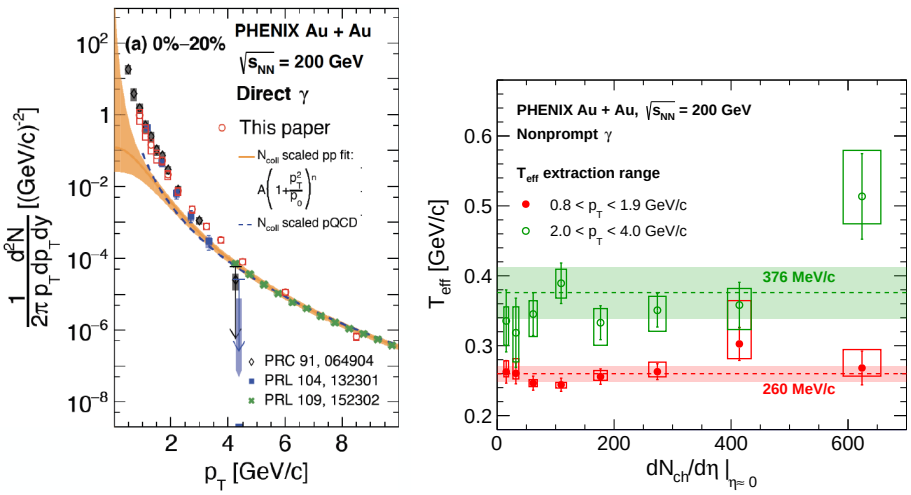

Figure 1. Left: direct-photon yield in central Au–Au collisions at $\sqrt{s_{\rm NN}} = 200\,\text{GeV}$, compared to prompt hard-scattering γ expectations [3]. Right: effective temperatures $T_{\rm eff}$ extracted from the non-prompt γ spectra in Au–Au collisions at $\sqrt{s_{\rm NN}} = 200\,\text{GeV}$ as a function of $\mathrm{d}N_{\rm ch}/\mathrm{d}\eta|_{\eta=0}$ [3].

in the left panel of Fig. 1 in central Au–Au collisions at $\sqrt{s_{\rm NN}} = 200\,\text{GeV}$. After subtracting the prompt γ contribution, the effective temperatures $T_{\rm eff}$, extracted from the non-prompt γ invariant yields, are above the deconfinement temperature and increase with the $p_{\rm T}$-range used in the fit procedure (see right panel of Fig. 1). There is no obvious variation of $T_{\rm eff}$ with $\mathrm{d}N_{\rm ch}/\mathrm{d}\eta|_{\eta=0}$, although the data do not exclude a small increase. Naively, high $p_{\rm T}$ thermal γs are expected to be emitted early during the collision at a time where the temperature of the medium is high. Nevertheless, effects due to the radial expansion of this medium have to be properly taken into account [7, 8]. Moreover, contributions from the pre-equilibrium phase, where the temperature is not well defined, may significantly modify this picture for $p_{\rm T} \geq 2.5\text{-}3\,\text{GeV}/c$ depending on $\sqrt{s_{\rm NN}}$ [9].

2.2 New results in heavy-ion collisions at RHIC and at the LHC

The PHENIX Collaboration presented preliminary results on v_2 of direct photons in Au–Au collisions at $\sqrt{s_{\rm NN}} = 200\,\text{GeV}$, fully consistent with their previous published measurements obtained with a 10 times smaller data sample [10]. A simultaneous description of the large direct-photon yield and v_2 remains challenging for models [1, 3] ("direct-photon puzzle").

The direct-photon invariant yield in central Pb–Pb collisions at $\sqrt{s_{\rm NN}} = 5.02\,\text{TeV}$ measured by ALICE [12] is shown in the left panel of Fig. 2. The data are described by calculations including prompt, pre-equilibrium and thermal photons [1], although the predictions tend to overestimate the yield by about one sigma. In the right panel of Fig. 2, the integrated $1 < p_{\rm T} < 3 - 5\,\text{GeV}/c$ direct-photon yield is displayed as a function of $\mathrm{d}N_{\rm ch}/\mathrm{d}\eta|_{\eta=0}$ for Pb–Pb collisions at the LHC, and Au–Au and pp collisions at RHIC. The inconsistency between the STAR and PHENIX results at RHIC remains unresolved to this day. At the LHC, the results are consistent with both the universal power-law scaling behaviour observed by PHENIX [2, 3], as well as a similar extrapolation of the STAR measurements. Predictions from a state-of-the-art model [1] underestimate PHENIX data with increasing discrepancy

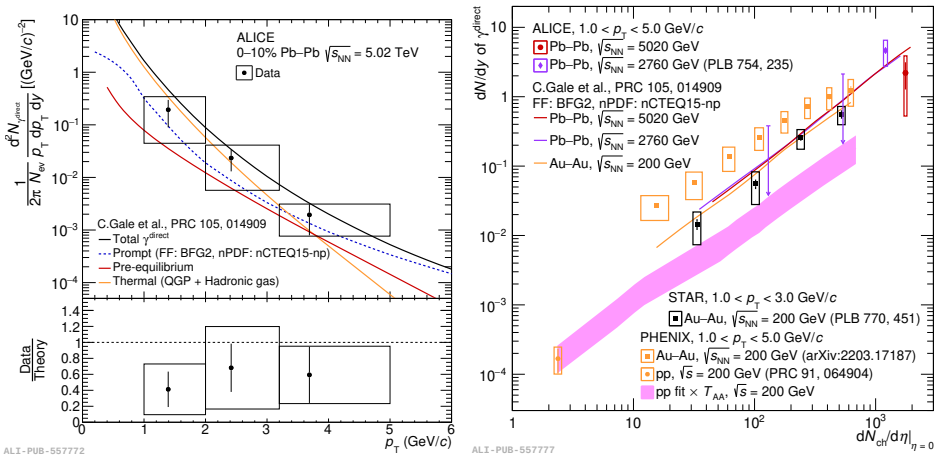

Figure 2. Left: direct-photon yield in central Pb–Pb collisions at $\sqrt{s_{\rm NN}} = 5.02$ TeV, compared with predictions [12]. Right: $p_{\rm T}$-integrated direct-photon yield in Pb–Pb, Au–Au and pp collisions as a function of $\mathrm{d}N_{\rm ch}/\mathrm{d}\eta|_{\eta=0}$ compared with calculations [12].

from semi-peripheral to peripheral Au–Au collisions, whereas it can fairly reproduce the STAR and ALICE measurements.

2.3 Proton-proton collisions at the LHC

The first measurement of direct photons at low $p_{\rm T}$ in small systems at the LHC was reported by the ALICE Collaboration. In the left panel of Fig. 3 the direct photon production cross section in minimum bias pp collisions at $\sqrt{s} = 13$ TeV is compared with two different calculations [13, 14]. The data are reproduced by predictions for prompt photons including or not including a thermal contribution. In the right panel of Fig. 3 the direct photon yield in minimum bias pp collisions is compared to the one in high-multiplicity pp events, where a significantly higher yield is observed. Such measurement provides input for calculations in small systems and the search for an onset of thermal radiation there.

3 Dileptons

In contrast to real photons, dileptons carry a mass ($m_{\rm ll}$). For $m_{\rm ll} > 1.2\,\mathrm{GeV}/c^2$, virtual photons are foreseen to originate from the partonic phase of the heavy-ion collision with a significant contribution of QGP thermal radiation. The slope of their $m_{\rm ll}$ distribution is predicted to carry information about the early temperature in the medium without distortion due to blueshift effect [15]. At lower $m_{\rm ll}$, dileptons can be used to study the in-medium modification of the ρ-meson spectral function related to mechanisms of chiral symmetry restoration [16].

3.1 Ag–Ag collisions at $\sqrt{s_{\rm NN}}$ = 2.42 and 2.55 GeV by HADES

A clear excess of $\mathrm{e^+e^-}$ pairs over the expected contribution of hadronic decays at freeze-out and the one from initial nucleon-nucleon interactions is observed by HADES in Ag–Ag collisions at $\sqrt{s_{\rm NN}} = 2.55$ and 2.42 GeV [18] for $m_{\rm ee} \geq 0.12\,\mathrm{GeV}/c^2$. The elliptic flow of dielectrons was measured differentially as a function of mass, pair transverse momentum,

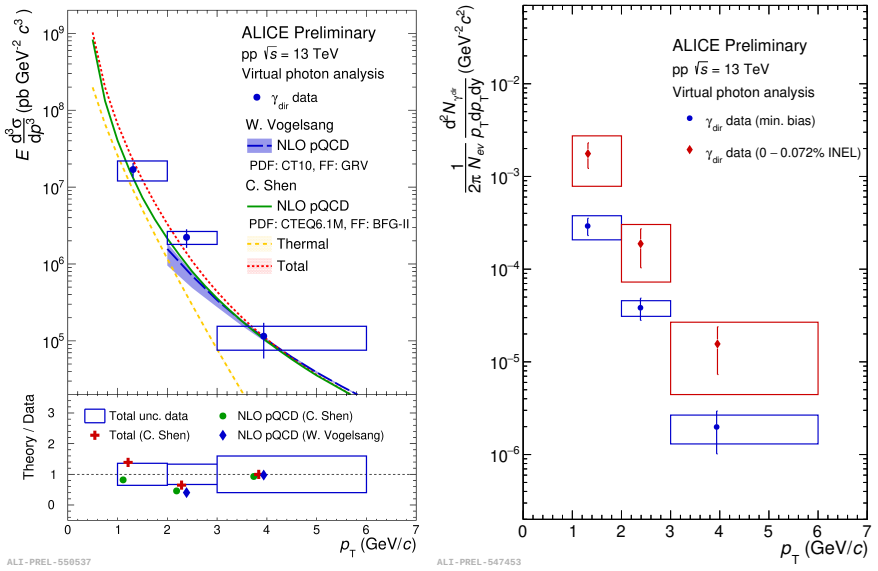

Figure 3. Left: direct-photon cross section in minimum bias pp collisions at $\sqrt{s} = 13$ TeV, compared with calculations [13, 14]. Right: direct-photon p_{T}-differential invariant yield in minimum bias and high-multiplicity pp collisions at $\sqrt{s} = 13$ TeV.

pair rapidity, and centrality. It is consistent with zero in the excess region in contrast to the negative v_2 for $\pi^{\pm}$ at this colliding energy due to spectator shadowing. These results confirm the penetrating nature of dileptons. The excess m_{ee}-spectrum has an exponential shape, in agreement with calculations for hadronic thermal radiation folded with a spacetime evolution of the fireball derived from a coarse-grained transport model [17].

3.2 Results from the RHIC Beam Energy Scan-II (BES-II) by STAR

The dielectron yields measured by STAR in Au–Au collisions at $\sqrt{s_{\mathrm{NN}}} = 7.7$, 14.6 and 19.6 GeV are shown in the left panel of Fig. 4. They are compared to a cocktail of hadronic decays at freeze-out (without ρ meson) and the expected contribution from the Drell-Yan process. An excess of $\mathrm{e^+e^-}$ signal is observed for $0.4 < m_{\mathrm{ee}} \leq 1\,\mathrm{GeV}/c^2$. The integrated excess yield in $0.4 < m_{\mathrm{ee}} \leq 0.75\,\mathrm{GeV}/c^2$ is corrected for acceptance and displayed as a function of $\sqrt{s_{\mathrm{NN}}}$ on the right panel of Fig. 4. Results from a previous analysis of the BES-I data in Au–Au collisions at $\sqrt{s_{\mathrm{NN}}} = 19$, 27, 39, 62.4 and 200 GeV [19] are also shown together with calculations including thermal production of ρ mesons with in-medium broadening spectral function and thermal radiation from the QGP (small in this mass range) [15]. The predictions can reproduce the data for $\sqrt{s_{\mathrm{NN}}} \geq 17.3$ GeV, whereas at lower energy the uncertainties are too large to make any quantitative statement. In this region the baryon density increases significantly and the temperature at chemical freeze-out decreases. Future experiments, like CBM and NA60+, will help to further investigate this region of the phase diagramm.

At higher mass ($1.2 < m_{\mathrm{ee}} \leq 2.7\,\mathrm{GeV}/c^2$) the published $\mathrm{e^+e^-}$ excesses from the BES-I analysis were compared for the first time with calculations for QGP thermal radiation using production rates up to next-to-leading order at finite μ_{B}, integrated over time with a realistic hydrodynamic model [11]. A good agreement is observed. More precise experimental data are nevertheless needed to exploit the full potential of such measurements.

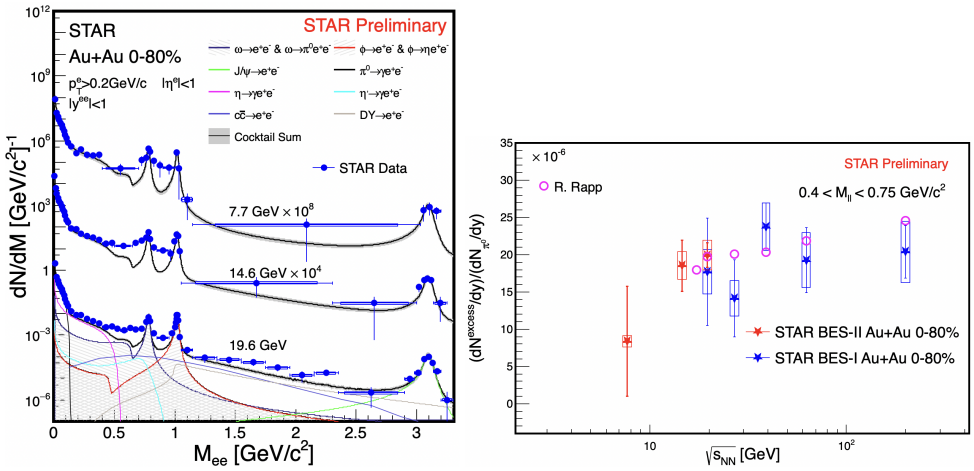

Figure 4. Left: dielectron yield in Au–Au collisions at $\sqrt{s_{\rm NN}}$ = 7.7, 14.6, 19.6 GeV, compared with a cocktail of background dielectrons (see text). Right: corresponding excess e^+e^- yield at low $m_{\rm ee}$ corrected for acceptance as a function of $\sqrt{s_{\rm NN}}$ compared to predictions.

3.3 Dielectrons in Pb–Pb and pp collisions at LHC energies by ALICE

The dielectron yield in central Pb–Pb collisions at $\sqrt{s_{\rm NN}}$ = 5.02 TeV measured by ALICE [12] is compared to two different cocktails of e^+e^- pairs from hadronic decays in the left panel of Fig. 5. The large background from correlated heavy-flavour hadron decays is estimated from dielectron measurements in pp collisions neglecting any initial state and medium effects (solid blue curve "Cocktail1") or calculated including information from single heavy-flavour decay electron measurements (dashed grey curve "Cocktail2", see [12] for more details). As of now no clear excess over the cocktails is observed. The e^+e^- yield is nevertheless consistent with calculations including additional contribution of thermal radiation from the hadronic and partonic phase (magenta and orange curves), although a tension of the order of 3σ is found for $0.5 < m_{\rm ee} < 0.8\,{\rm GeV}/c^2$.

The ALICE data from the LHC Run 3 will provide more statistics, up to a factor 100 for Pb–Pb collisions, and a (better) separation of the heavy-flavour background from prompt e^+e^- pairs including thermal radiation. For this purpose, the distance-of-closest approach (DCA) of the electron and positron to the reconstructed collision point can be used to define a pair $\mathrm{DCA}_{\rm ee}^{\rm 3D}$. Analysis of the first pp collisions at $\sqrt{s_{\rm NN}}$ = 13.6 TeV shows that the continuum-like heavy-flavour contribution can be nicely separated from the light-flavour and prompt J/Ψ decays by selecting dielectrons with large DCA (see right panel of Fig. 5).

4 Summary and Outlook

Electromagnetic probes provide the unique possibility to gain undistorded information about the properties and space-time evolution of the medium created in heavy-ion collisions. Direct photons are measured with increasing precision at RHIC and at the LHC. However, discrepancies between results from different experiments (STAR and PHENIX) need to be resolved in order to give clear inputs to model calculations and to understand the yield and v_2 of direct photons simultaneously. Measurements of the dilepton production at very different $\mu_{\rm B}$ and T are carried out. Most of them still suffer from large uncertainties, although theoretical works

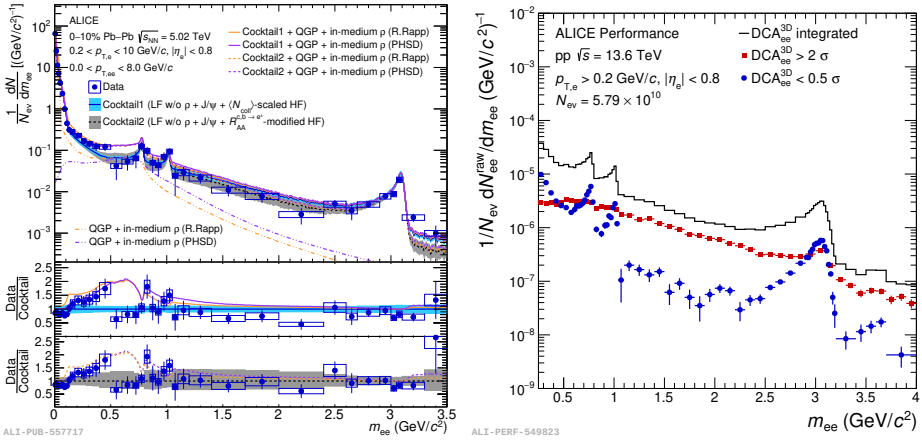

Figure 5. Left: dielectron yield in central Pb–Pb collisions at $\sqrt{s_{\rm NN}}$ = 5.02 TeV, compared with the expected e^+e^- contributions from known hadronic decays, including or not including medium effects for heavy-flavour (see text), and two predictions for thermal radiation from the medium. Right: raw dielectron spectra for different requirement on the pair DCA_{ee}^{3D} in pp collisions at $\sqrt{s_{\rm NN}}$ = 13.6 TeV.

show a large potential for more differential dielectron studies. Therefore a huge experimental efforts is ongoing in order to make such measurements possible with future upgrades and planned experiments (HADES, STAR, CBM, NA60+, ALICE and ALICE 3).

References

[1] C. Gale, J.-F. Paquet, B. Schenke, and C. Shen, Phys. Rev. C **105**, 014909 (2022)
[2] PHENIX Collaboration, Phys. Rev. C **107**, 024914 (2023)
[3] PHENIX Collaboration, arXiv:2203.17187
[4] STAR Collaboration, Phys. Lett. B **770**, 451 (2017)
[5] ALICE Collaboration, Phys. Lett. B **754**, 235 (2016)
[6] A. Marin for the ALICE Collaboration, Hard Probes 2023, arXiv:2308.02401
[7] C. Shen, U. W. Heinz, J.-F. Paquet and C. Gale, Phys. Rev. C **89**, 044910 (2014)
[8] J.-F. Paquet, arXiv:2305.10669
[9] O. Garcia-Montero, A. Mazeliauskas, P. Plaschke, and S. Schlichting, arXiv:2308.09747
[10] PHENIX Collaboration, Phys. Rev. C **94**, 064901 (2016)
[11] J. Churchill, L. Du, C. Gale, G. Jackson, and S. Jeon, arXiv:2311.06951
[12] ALICE Collaboration, arXiv:2308.16704
[13] L. E. Gordon and W. Vogelsang, Phys. Rev. D **48**, 3136 (1993)
[14] C. Shen *et al.*, Phys. Rev. C **95**, 014906 (2017)
[15] R. Rapp and H. van Hees, Phys. Lett. B **753**, 586 (2016)
[16] P. M. Hohler and R. Rapp, Phys. Lett. B **731**, 103 (2014)
[17] HADES Collaboration, Nature Phys. **15**, 1040 (2019)
[18] N. Schild for the HADES Collaboration, PoS FAIRness2022, 053 (2023)
[19] STAR Collaboration, Phys. Rev. C **107**, 061901 (2023)